International Journal of Minerals, Metallurgy and Materials
Volume 21, Number 8, August 2014, Page 785
DOI: 10.1007/s12613-014-0972-z

Microstructure and texture evolution in commercial-purity Zr 702 during cold rolling and annealing

Min Ma, Ming-he Li, Yuan-biao Tan, Hui Yuan, and Wen-chang Liu

Key Laboratory of Metastable Materials Science and Technology, College of Materials Science and Engineering, Yanshan University, Qinhuangdao 066004, China
(Received: 22 December 2013; revised: 5 March 2014; accepted: 10 March 2014)

Abstract: Microstructure and texture evolution in commercial-purity Zr 702 during cold rolling and annealing was investigated by optical microscopy, transmission electron microscopy, and X-ray diffraction. The results showed that crystallographic slip was the predominant deformation mechanism in the early stage of deformation. Deformation twins started to form when the rolling reduction was larger than 38.9%; both the dislocation density and the number of twins increased with increasing rolling reduction. The initial texture of the Zr 702 plate consisted of the basal fiber component. During cold rolling the strength of the basal fiber first decreased and then increased with increasing rolling reduction. The cold-rolled sheets were fully recrystallized after being annealed at 550°C. The recrystallization temperature and the size of recrystallized grains decreased with increasing rolling reduction. A larger rolling reduction resulted in a higher grain growth rate when the annealing temperature increased from 550°C to 700°C. The recrystallization texture was characterized by a major basal fiber and a minor $\{01\bar{1}3\}\langle 2\bar{1}\bar{1}0\rangle$ component. The strength of the recrystallization texture increased with increasing rolling reduction.

Keywords: zirconium; cold rolling; annealing; microstructure; texture; recrystallization

1. Introduction

Zirconium alloys have been widely used in the nuclear industry because of their low probability of neutron capture and excellent resistance to water or vapor corrosion in a high-temperature and high-pressure environment. In general, excellent mechanical properties are required for applications in nuclear reactors. The mechanical properties of materials depend on the microstructure and texture developed during manufacturing processes. Zirconium and its alloys have a hexagonal close-packed (HCP) structure and various operating slip and twinning systems, depending on the orientation of the crystals. Their relevant physical and mechanical properties exhibit strong anisotropy because of the presence of crystallographic texture. Control of their microstructure and texture is therefore important.

Recrystallized zirconium alloys are known to be suitable for nuclear applications because of their low irradiation growth [1] and high irradiation creep resistance [2–3]. Numerous researchers have attempted to understand the evolution of microstructure and texture during the cold rolling and annealing of Zr alloys [4–17]. Castelnau *et al.* [17] studied the texture development of Zr 702 with different initial textures. They observed that the orientation dependence of the activated slip systems was strongly influenced by the texture and that intracrystalline hardening did not substantially affect the development of texture. Chun *et al.* [6] reported that the addition of Mo resulted in weakening of the normal basal texture and promoted a texture shift during annealing in Zr–Nb alloys. Kumar *et al.* [7] studied the deformation texture after unidirectional and cross rolling of Zr–2.5wt%Nb with two distinct starting microstructures. They observed that the texture in the two-phase structure material insignificantly changed, whereas noticeable textural changes occurred in the single-phase structure material. Vanitha *et al.* [12] investigated the recrystallization texture development in single-phase Zircaloy-2. They observed an increase in texturing during the initial stages of recrystallization and a decrease beyond 20%–24% recrystallization. In

Corresponding author: Wen-chang Liu E-mail: wcliu@ysu.edu.cn

this study, Zr 702 plates were cold rolled to different reductions and then annealed at different temperatures for 1 h. The evolution of the microstructure and texture during cold rolling and annealing was investigated by optical microscopy, transmission electron microscopy (TEM), and X-ray diffraction.

2. Experimental

The material used in this study was commercial-purity Zr 702. The thickness of the as-received hot-rolled plates was 9.3 mm. Table 1 lists the chemical composition of Zr 702. The as-received plates were annealed in a vacuum furnace at 600°C for 2 h, resulting in an average grain size of 8.46 μm. The annealed plates were subsequently cold rolled to different reductions on a laboratory rolling mill with rolls having a diameter of 230 mm using a rolling speed of 0.4 m/s. The plates were rolled by alternating the top and bottom sides during multipass rolling. To study the annealing behavior of Zr 702, the cold-rolled sheets of various reductions were annealed in a vacuum furnace at different temperatures in the range of 350°C to 700°C for 1 h, followed by furnace cooling.

Table 1. Chemical composition of Zr 702 wt%

Hf	Fe	Cr	C	N	H	Zr
1.6	0.09	0.012	0.02	<0.01	0.001	Bal.

Optical microscopy and TEM were performed on the cross sections of the rolled samples in the longitudinal direction. Specimens for optical microscopy were mechanically polished and chemically etched using a solution of 10vol% hydrofluoric acid (HF), 45vol% nitric acid (HNO_3), and 45vol% distilled water (H_2O). Optical micrographs were taken under polarized light to examine the evolution of microstructures. The deformation microstructure was examined using a JEM–2010 transmission electron microscope. The specimens were thinned to 40 μm and twin-jet electro-polished in a solution of 10vol% perchloric acid and 90vol% ethanol at 15 V and −30°C. A Vickers hardness tester was used to measure the hardness with a load of 300 g to evaluate the extent of recovery and recrystallization. At least five hardness measurements were performed for each condition.

The texture measurements were performed in the center layer of the cold-rolled and annealed sheets. Using Cu K_α radiation, five incomplete pole figures (0002), $(10\bar{1}0)$, $(10\bar{1}1)$, $(10\bar{1}2)$, and $(11\bar{2}0)$ were measured up to a maximum tilt angle of 75° by the Schulz back-reflection method. The orientation distribution functions (ODFs) were calculated from the five incomplete pole figures using TexTools software. Euler angles were represented with reference to a crystal coordinate system of $X = [2\bar{1}\bar{1}0]$, $Y = [0\bar{1}10]$, and $Z = [0001]$.

3. Results

3.1. Evolution of microstructure and texture during cold rolling

3.1.1. Microstructure

Fig. 1 shows the optical micrographs of the longitudinal sections of the cold-rolled Zr 702 with various reductions. The starting material is comprised of equiaxed single-phase α-Zr with an average grain size of 8.46 μm (Fig. 1(a)). During the cold rolling, the grains were gradually elongated along the rolling direction (RD). At 38.9% rolling reduction, the deformation microstructure was heterogeneous due to local discrepancies in the slip activity, depending on grain orientation. The macroscopic shear bands of approximately 35° to RD or microbands started to appear. The number of shear bands increased with increasing rolling reduction. At 71.0% rolling reduction, the microstructure became much more refined and the macroscopic shear banding was more evident (Fig. 1(d)).

Fig. 2 details the evolution of the microstructure during the cold rolling, which was characterized by TEM. At 20.4% rolling reduction, some tangled dislocations were observed, although no deformation twinning was evident (Fig. 2(a)). This result indicates that crystallographic slip is the predominant deformation mechanism in the early stage of deformation. At 38.9% rolling reduction, a few deformation twins were observed (Fig. 2(c)). The dislocation density increased with increasing rolling reduction, while the size of the dislocation cells decreased (Figs. 2(a), 2(b), and 2(d)). The number of twins also increased with increasing rolling reduction (Figs. 2(c), 2(e), and 2(g)). At 71.0% rolling reduction, the microstructure exhibited a fine lamellar structure with a thickness of 100–150 nm, in which a high dislocation density was observed (Fig. 2(f)). The twin boundaries were marked by wavy boundaries (Fig. 2(h)), suggesting that the ideal twin–matrix orientation relationship was destroyed through the deformation via slip in both the twin and the matrix to accommodate the deformation imposed by twin formation [18].

3.1.2. Rolling texture

Fig. 3 shows the measured (0002), $(10\bar{1}1)$, and $(10\bar{1}2)$ pole figures of Zr 702 cold rolled to various reductions. The (0002) pole figure of the initial plate did not exhibit a bi-

modal distribution along the transverse direction (TD); it rather exhibited a basal texture with the maximum pole density parallel to the ND. During the rolling, the distribution of the basal poles did not substantially change. Similarly, the cold rolling reduction had no noticeable effect on the distribution of the other pole figures.

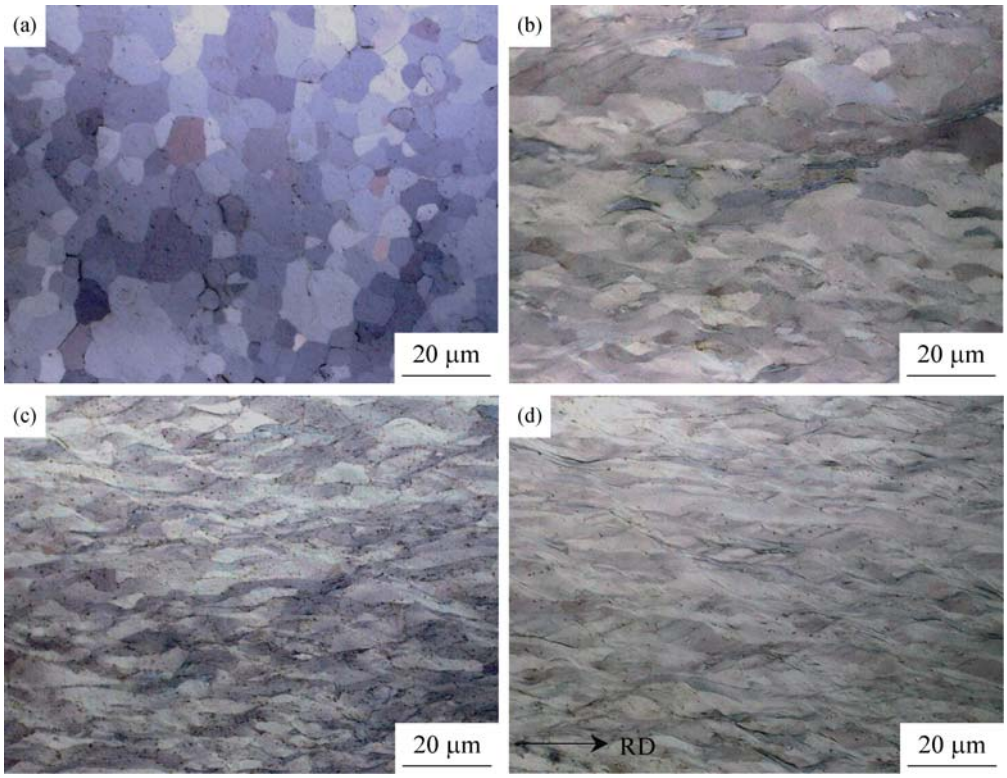

Fig. 1. Optical micrographs showing the microstructure of Zr 702 cold rolled to reductions of (a) 0%, (b) 38.9%, (c) 58.3%, and (d) 71.0%.

The ODFs of the Zr 702 cold rolled to various reductions are shown in Fig. 4. The texture of the initial plate consisted mainly of the basal fiber {0001}<*uvtw*> (φ_1 = 0°–90°, Φ = 0°, and φ_2 = 0°). During the rolling, the basal fiber changed only slightly; i.e., the relative intensities at the specific fiber location changed, but the overall fiber appearance remained approximately the same. To clearly reveal the change in the basal fiber during the rolling, the orientation density $f(g)$ along the line of Φ = 0° at the plane of φ_2 = 0° is plotted in Fig. 5(a) for different cold-rolled sheets. It is noted that the strength of the basal fiber decreased when the plate was cold rolled to 20.4%, and then increased with further increasing rolling reduction. In the initial plate, the maximum density was located at the {0001}<2 $\bar{1}$ $\bar{1}$ 0> orientation, which was the main texture component. After 71.0% rolling reduction, the location of the maximum density shifted to the {0001}<10 $\bar{1}$ 0> orientation. Fig. 5(b) shows the orientation density $f(g)$ along the line of φ_1 = 0° at the plane of φ_2 = 0°. The density of the {01 $\bar{1}$ 3}<2 $\bar{1}$ $\bar{1}$ 0> orientation decreased with increasing rolling reduction.

3.2. Recrystallization and recrystallization texture

3.2.1. Recrystallization

Figs. 6 to 8 show the microstructural changes in the cold-rolled Zr 702 sheets with respect to the annealing temperature. For the 20.4% cold-rolled sheet (Fig. 6), the slightly elongated grains hardly changed at annealing temperature less than 450°C. Some small equiaxed grains were observed at 500°C. After being annealed at 550°C, the cold-rolled sheet was fully recrystallized with equiaxed coarse grains. The recrystallized grains grew with further increasing the annealing temperature. For the 58.3% and 71.0% cold-rolled sheets, the microstructures consisted of equiaxed fine grains after the sheets were annealed at 500°C. The effect of the rolling reduction on the recrystallized grains is shown in Fig. 9. At 550°C, the size of the recrystallized grains decreased with increasing rolling reduction. The grain growth rate depended strongly on the rolling reduction. The recrystallized grains grew more rapidly for larger reductions than for small reductions when the annealing tem-

perature increased from 550°C to 700°C. At 700°C, the size of the recrystallized grains decreased slightly with increasing rolling reduction.

The extent of recrystallization is often studied by measurements of hardness. Fig. 10 shows the variation of Vickers hardness with the annealing temperature for Zr 702 cold rolled to various reductions. The hardness did not exhibit a notable change at low annealing temperatures, which suggests that the extent of recovery of the cold-rolled Zr 702 was limited because of its HCP structure and low stacking fault energy, which is consistent with the experimental observations of Zr-4 [5]. The hardness decreased substantially as the annealing temperature increased from 400°C to 550°C, indicating the occurrence of recrystallization. A comparison of the hardness–temperature curves reveals that the recrystallization temperature decreased with increasing rolling reduction.

3.2.2. Recrystallization texture

Fig. 11 shows the measured (0002), $(10\bar{1}1)$, and $(10\bar{1}2)$ pole figures of the Zr 702 plates cold rolled to 38.9% and 71.0% reductions and then annealed at 600°C for 1 h. Compared to the pole figures of the cold-rolled samples, the (0002) pole figure of the recrystallized samples exhibited a bimodal distribution along the TD. For the 38.9% cold-rolled sheet, the maximum pole density was located at 25° toward the TD from the ND, whereas the position of the

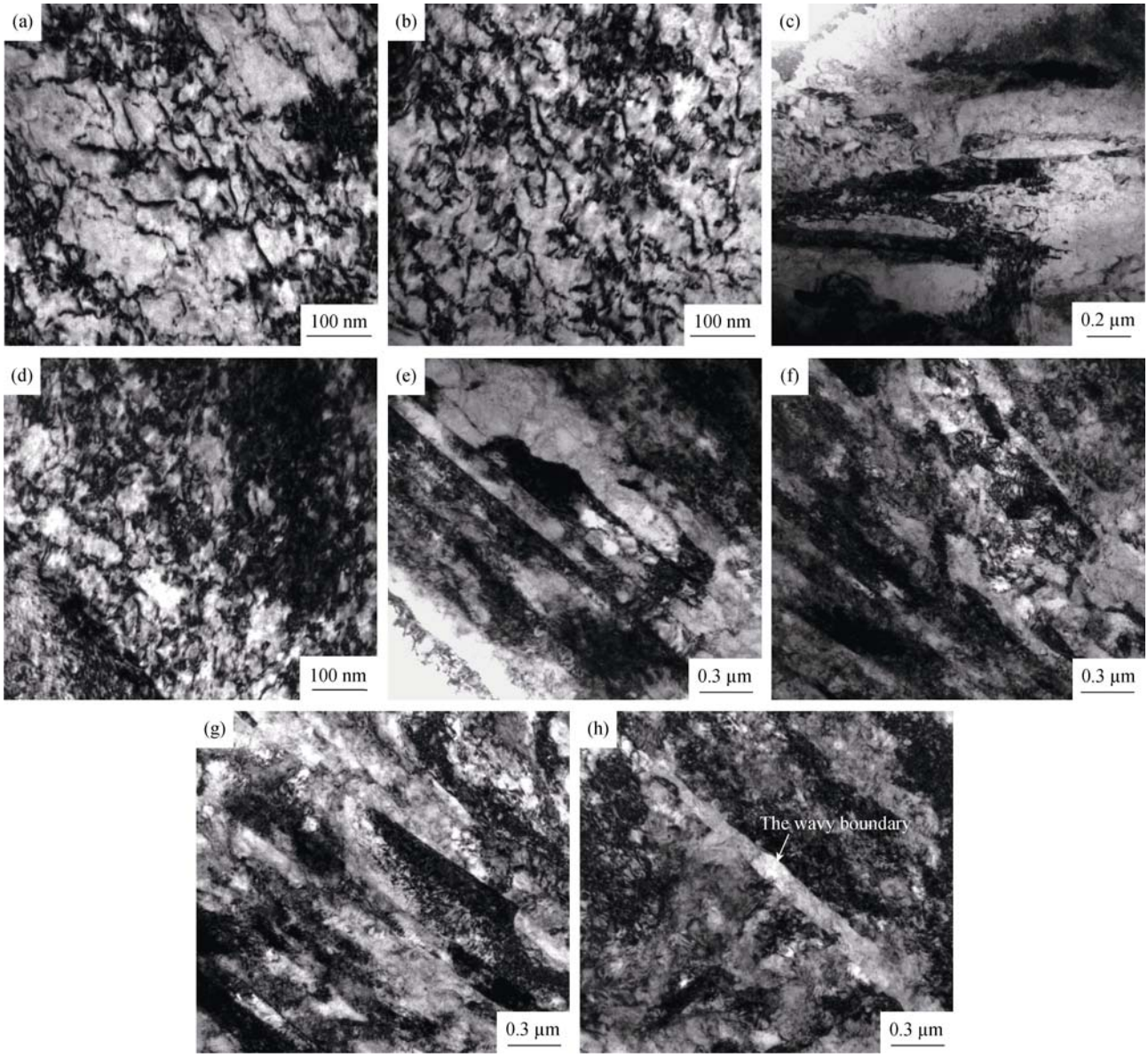

Fig. 2. TEM micrographs showing the microstructure of Zr 702 cold rolled to reductions of (a) 20.4%, (b) and (c) 38.9%, (d) and (e) 58.3%, and (f) to (h) 71.0%.

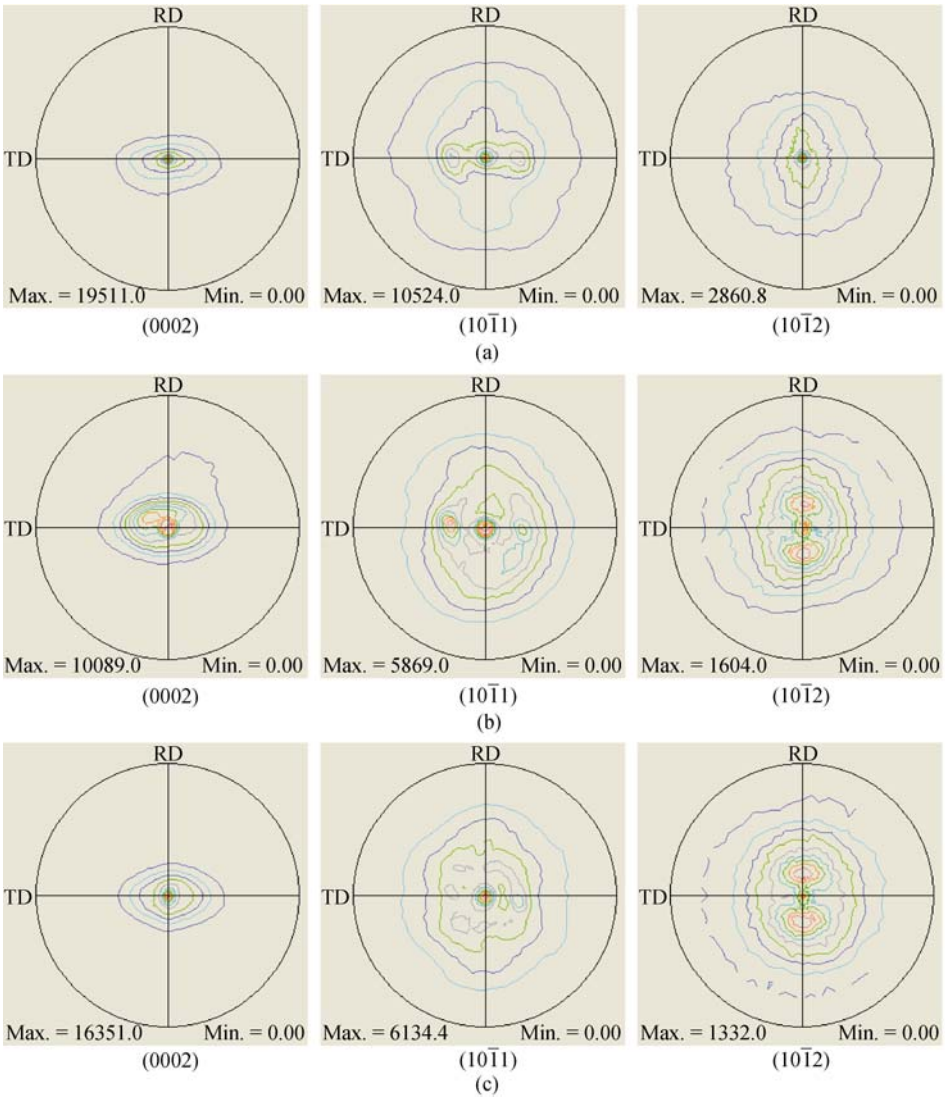

Fig. 3. Measured pole figures of Zr 702 cold rolled to (a) 0%, (b) 38.9%, and (c) 71.0% reductions.

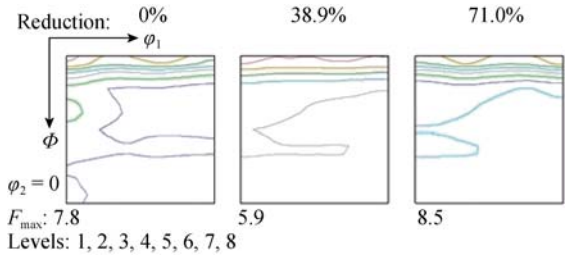

Fig. 4. Textures of Zr 702 cold rolled to 0%, 38.9%, and 71.0% reductions (F_{max} is the biggest orientation strength of ODF).

maximum density shifted to 15° from the ND in the case of the 71.0% cold-rolled sheet. The ODFs of the recrystallized specimens are presented in Fig. 12. The recrystallization texture was characterized by a major basal fiber (0001)<2$\bar{1}$ $\bar{1}$0> and minor components {01$\bar{1}$3}<2$\bar{1}$ $\bar{1}$0> and {$\bar{1}$2$\bar{1}$5}<10$\bar{1}$0>. This texture is similar to the results previously reported for rolled and annealed Zr when the annealing temperature was less than approximately 600°C [19]. A comparison of Fig. 12 with Fig. 4 reveals that the recrystallization texture remained the same type as the deformation texture, but the texture strength obviously decreased after complete recrystallization. The recrystallization texture of the cold-rolled Zr 702 sheets depended on the rolling reduction. The texture strength increased with increasing rolling reduction.

Fig. 13 shows the orientation density $f(g)$ along the lines of $\Phi = 0°$ and $\varphi_1 = 0°$ at the plane of $\varphi_2 = 0°$. A comparison of Fig. 13 with Fig. 5 reveals that the density of the {01$\bar{1}$3}<2$\bar{1}$ $\bar{1}$0> orientation increased after the recrystallization annealing and the intensities of orientations along the basal fiber decreased. These results suggest that the recrystallization component {01$\bar{1}$3}<2$\bar{1}$ $\bar{1}$0> was formed at the expense of the basal fiber.

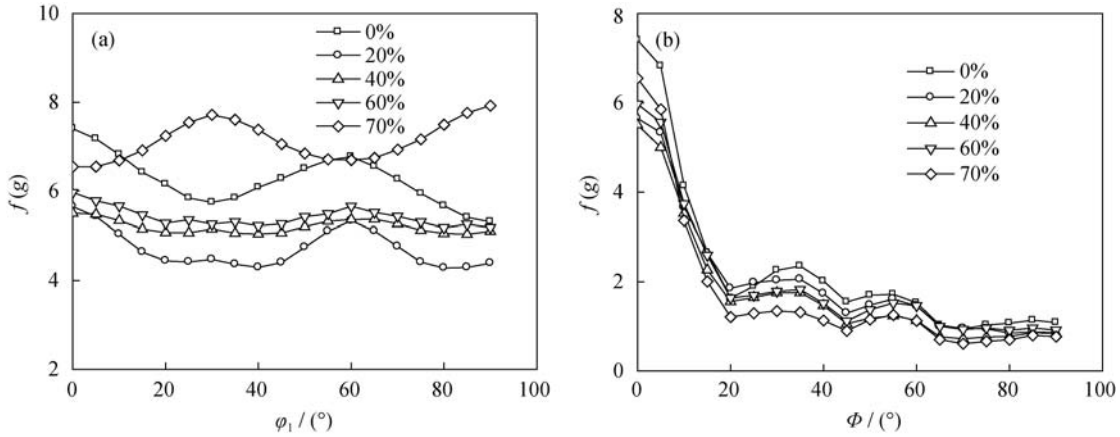

Fig. 5. Variations in orientation density $f(g)$ along the line of (a) $\Phi = 0°$ and (b) $\varphi_1 = 0°$ at the plane of $\varphi_2 = 0°$ for different cold-rolled samples.

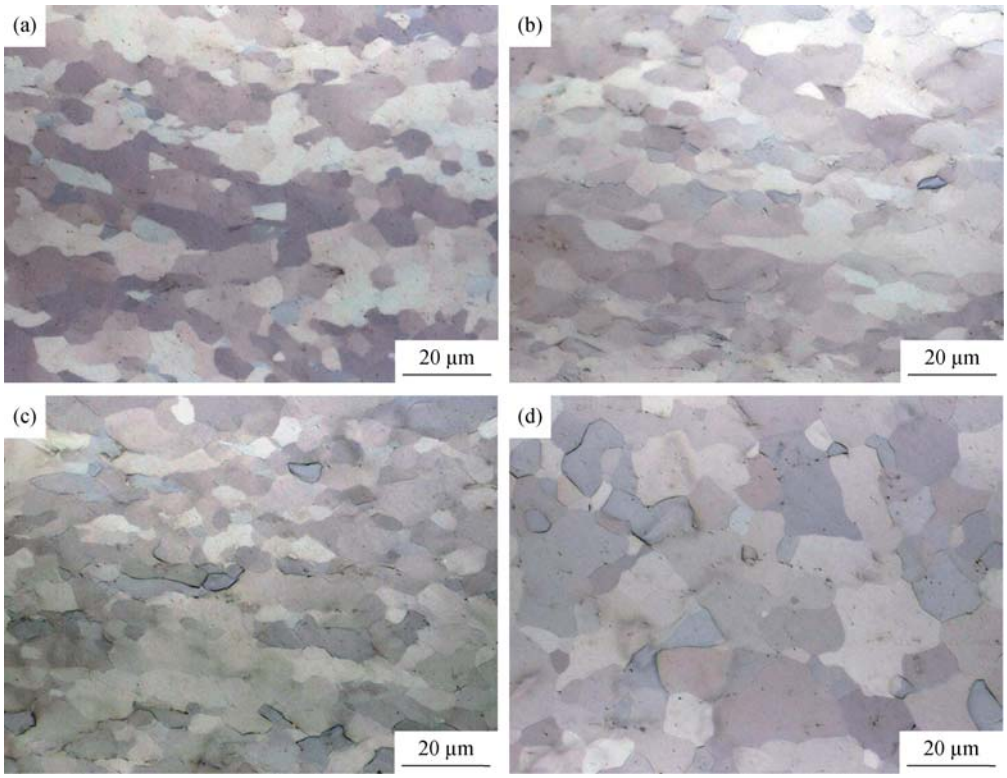

Fig. 6. Microstructures of Zr 702 cold rolled to 20.4% reduction and then annealed at (a) 400°C, (b) 450°C, (c) 500°C, and (d) 550°C.

4. Discussion

During the cold-rolling process, Zr polycrystals started to deform by dislocation glide. A number of dislocations were observed in the 20.4% cold-rolled sheet, indicating that crystallographic slip was the predominant deformation mechanism in the early stages of deformation. Several slip systems are known to be active in Zr. At room temperature, slip occurs preferentially in $\{10\bar{1}0\}\langle 11\bar{2}0\rangle$ prismatic systems [20]. In addition, numerous experimental studies have shown the occurrence of the first-order pyramidal slips $\{10\bar{1}1\}\langle 11\bar{2}0\rangle$ and $\{10\bar{1}1\}\langle \bar{2}113\rangle$ [21] and $\{10\bar{1}\bar{1}\}\langle 11\bar{2}3\rangle$ [22], the latter of which allows a crystal contraction along the *c*-axis. Prismatic slip is active over the whole temperature range, whereas pyramidal slip is active at and above room temperature [23–24]. Several works have demonstrated the possible activation of basal slip $\{0001\}\langle 11\bar{2}0\rangle$ [25]. Basal slip at room temperature is associated with basal screw dislocations and the cross slip

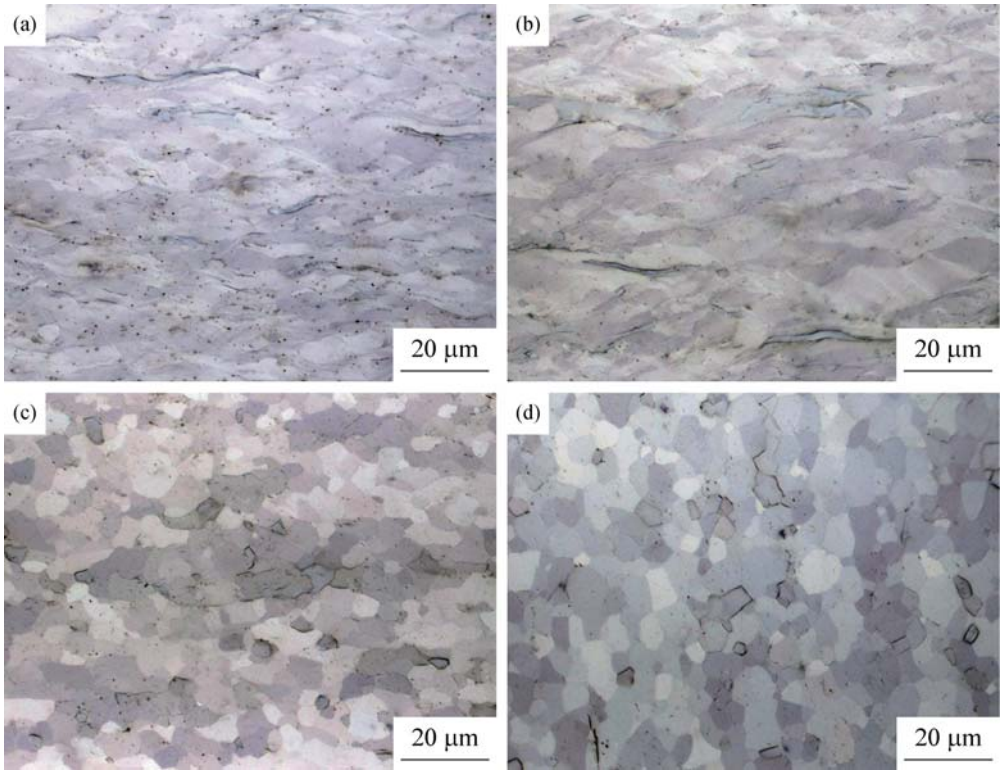

Fig. 7. Microstructures of Zr 702 cold rolled to 58.3% reduction and then annealed at (a) 400°C, (b) 450°C, (c) 500°C, and (d) 550°C.

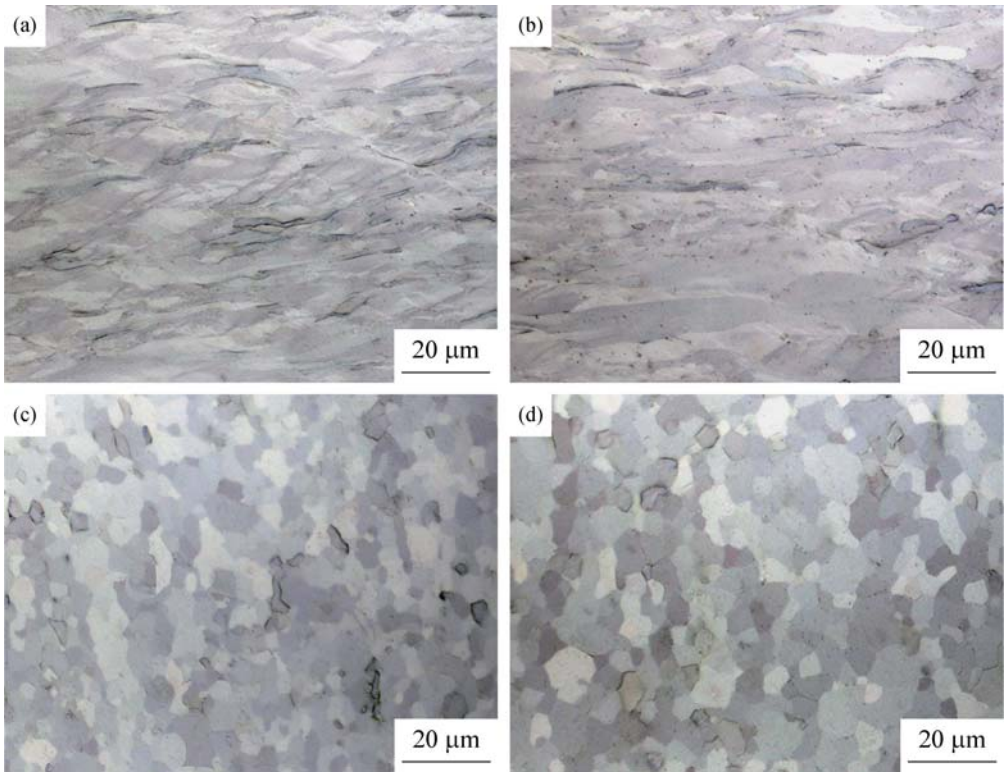

Fig. 8. Microstructures of Zr 702 cold rolled to 71.0% reduction and then annealed at (a) 400°C, (b) 450°C, (c) 500°C, and (d) 550°C.

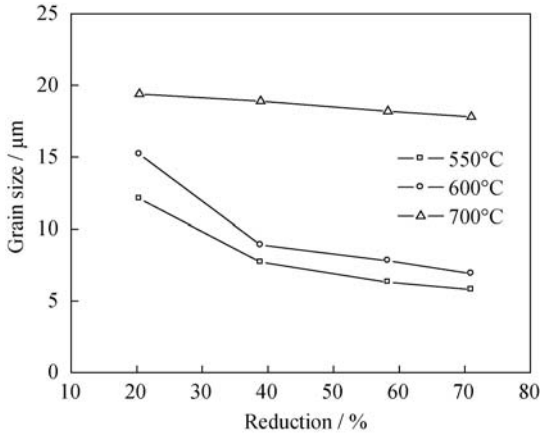

Fig. 9. Variation in grain size with rolling reduction for the cold-rolled sheets annealed at different temperatures.

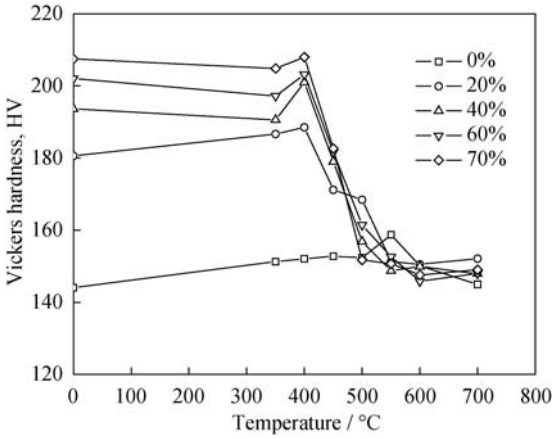

Fig. 10. Variation in Vickers hardness with annealing temperature for Zr 702 cold rolled to different reductions.

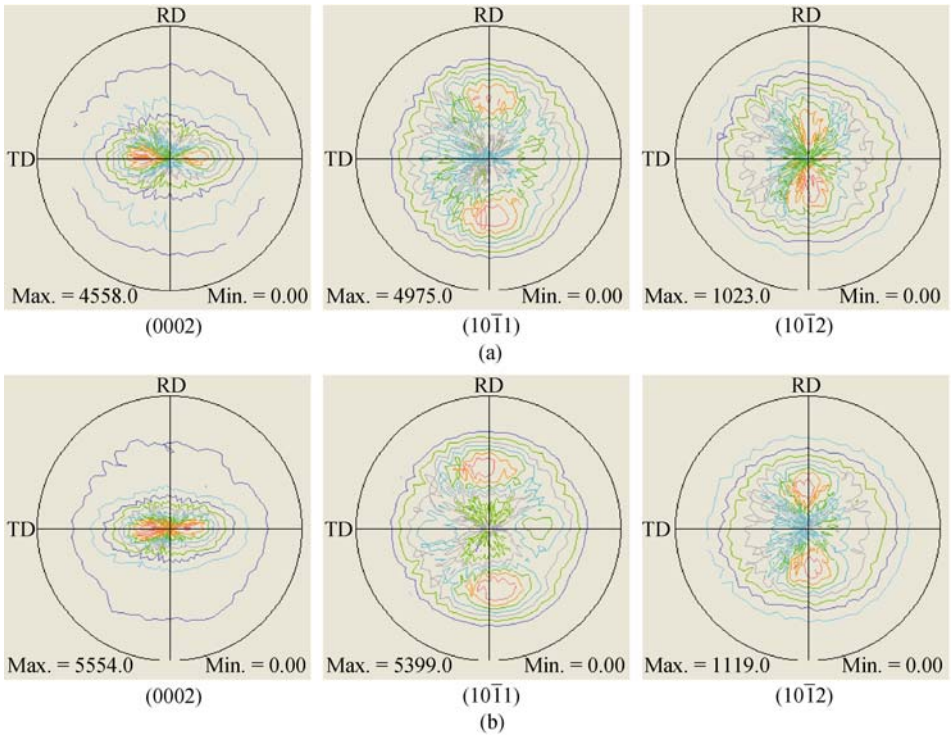

Fig. 11. Measured pole figures of Zr 702 cold rolled to (a) 38.9% and (b) 71.0% reductions and then annealed at 600°C for 1 h.

between basal and prismatic planes [26]. Basal slip is also related to the formation of a kink band [27]. However, the symmetry of the lattice and the availability of slip systems in HCP metals are less than in other metals. Under these conditions, slip cannot continue as the only deformation mode and twinning becomes significant. At a reduction of 38.9%, a few twins were observed, and the number of twins increased with increasing rolling reduction. This observation is consistent with a previous investigation where the critical strain to form twins was reported to occur at approximately 25% reduction in pure Zr [19].

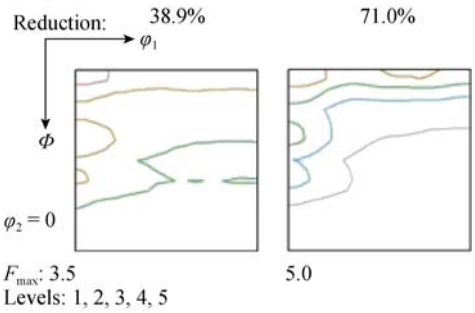

Fig. 12. Textures of Zr 702 cold rolled to 38.9% and 71.0% reductions and then annealed at 600°C for 1 h.

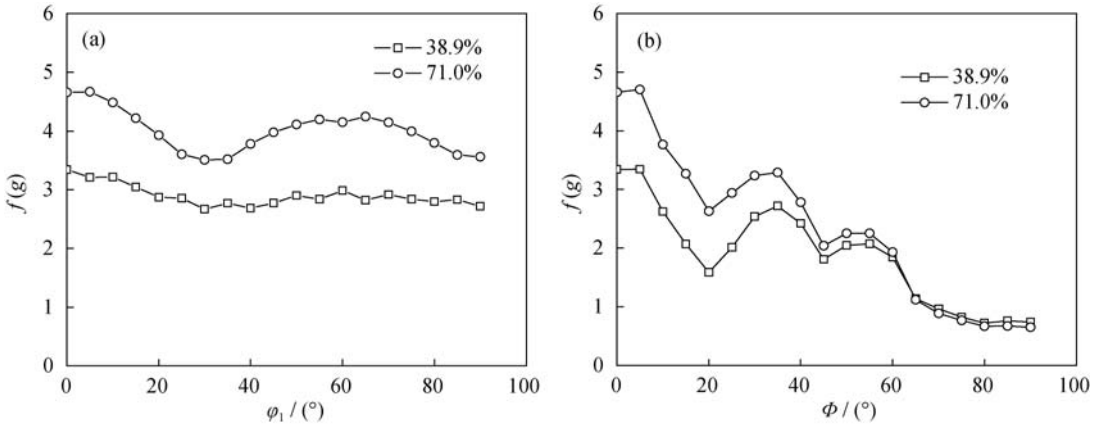

Fig. 13. Variation in orientation density *f*(*g*) along the line of (a) $\Phi = 0°$ and (b) $\varphi_1 = 0°$ at the plane of $\varphi_2 = 0°$ for Zr 702 cold rolled to 38.9% and 71.0% reductions and then annealed at 600°C for 1 h.

Dislocations and twins play an important role in the plastic deformation and hardening of Zr. The main twinning systems observed in zirconium are tensile twins in the $\{10\bar{1}2\}<10\bar{1}\bar{1}>$ system and compressive twins in the $\{11\bar{2}2\}<11\bar{2}\bar{3}>$ system [28]. Tensile twinning accommodates the elongation along the *c*-axis of the crystal, whereas compressive twinning accommodates the *c*-axis contraction [29]. Zhu *et al.* [8] used orientation imaging microscopy (OIM) to study the microstructure of a Zr–2Hf alloy sheet deformed by plane strain compression. They observed that the most frequent twins are the $\{10\bar{1}2\}<10\bar{1}\bar{1}>$ and $\{11\bar{2}1\}<11\bar{2}\bar{6}>$ systems, whereas the $\{11\bar{2}2\}<11\bar{2}\bar{3}>$ and $\{10\bar{1}1\}<10\bar{1}\bar{2}>$ systems are less frequent. The formation of deformation twins depends strongly on the exact orientation of the deformed grains [25]. When the *c*-axis lies closer to the TD, twinning is often active, producing a small extension along TD and a small compression along RD within the twinned grain.

The initial Zr 702 plate annealed at 600°C exhibited a strong basal texture. During subsequent cold rolling of the plate, the density of orientations along the basal texture changed, although the initial basal texture did not substantially change. This result is similar to that reported for Zr–2.5wt%Nb alloy [7]. Data in Fig. 5 further indicate that the strength of the basal fiber decreased when the initial sheet was cold rolled to 20.4% and then increased with further increasing rolling reduction. The increase in strength of the basal texture can be attributed to the enhanced probability of twinning, which was produced by large deformation [6]. Moreover, the maximum position of the basal texture changed from the $<2\bar{1}\bar{1}0>$ orientation in the initial state to the $<10\bar{1}0>$ orientation in the 70% rolled state. The $<10\bar{1}0>$ preferred orientation is typical of the deformed state. This result is in agreement with the results of previous investigations on cold-rolled Zr alloys [8].

The cold-rolled Zr 702 sheets had a high stored energy derived mainly from the accumulation of dislocations and the formation of deformation twinning. Recovery and recrystallization occurred during annealing of the cold-rolled sheets, which led to a decrease in strength and hardness. Fig. 10 reveals that the hardness of the cold-rolled sheets did not substantially change after they were annealed at low annealing temperatures. This result indicates that the extent of dislocation recovery is limited because of the HCP structure and low stacking fault energy. As the annealing temperature further increased, the cold-rolled sheet started to recrystallize, leading to a substantial decrease in hardness. The nucleation of the recrystallized grains first occurred at various microstructural inhomogeneities such as localized shear bands and twins in the severely deformed area and then continued into the somewhat less deformed areas. TEM observations indicated that the twins essentially acted as linear features that block dislocation activity in the direction perpendicular to the twin thickness. As a result, high stored energies and localized matrix rotations occurred in the vicinity of the twins that act as potential nucleation sites for recrystallized grains [30]. Zhu *et al.* [8] studied the recrystallization mechanism of Zr–2Hf alloy by *in situ* high-voltage electron microscopy and electron back-scattered diffraction. They observed that the recrystallized grains formed through the rearrangement of dislocation cells into subgrains, the formation of nuclei through growth or coalescence of subgrains, and the growth of nuclei by high-angle boundary migration. The recrystallization kinetics of the cold-rolled Zr 702 was determined via hardness measurements. The Johnson–Mehl–Avrami–Kolmogorov exponent obtained is less than 1, which implies that the cold deformation of Zr 702 led to a non-uniform distribution of stored energy and re-

crystallization might occur by heterogeneous site-saturated and constant-rate nucleation at localized shear bands and twins [31].

The recrystallization texture of the cold-rolled Zr 702 sheets was characterized by the basal fiber and the $\{01\bar{1}3\}<2\bar{1}\bar{1}0>$ component. In the case of the 38.9% cold-rolled sheet, although the densities of orientations along the basal fiber decreased and the density of the $\{01\bar{1}3\}<2\bar{1}\bar{1}0>$ orientation increased after the recrystallization annealing, its recrystallization texture remained the same type as the deformation texture. This similarity indicates that the oriented nucleation plays an important role in determining the final recrystallization texture. The nuclei evolved from dislocation cells present in the as-deformed microstructure. During the growth of nuclei by high-angle boundary migration, the global texture of the material did not substantially change. Gerspach *et al.* [11] studied the texture stability during the recrystallization of cold-rolled Zr 702. They observed that the recrystallization texture of the cold-rolled sheets remained stable, with a very limited decrease of the texture index. This behavior is attributed to the formation of nuclei in a non-oriented manner and to a lack of significant selection of orientation during their growth [11]. However, in the case of the 71% cold-rolled sheet, the maximum position of the basal texture changed from $(0001)<10\bar{1}0>$ orientation in the deformation texture to $(0001)<11\bar{2}0>$ orientation in the recrystallization texture by 30° rotation around the *c*-axis. This change indicates that oriented growth is promoted by orientation pinning. The growth of recrystallized grains will be inhibited by contact with grains in a deformation matrix with similar orientations [11,32]. After serious plastic deformation, the rolling texture became stronger, and hence the effect of orientation pinning became so significant that the maximum position of the basal texture changed.

5. Conclusions

Microstructure and texture evolution during the cold rolling and annealing of Zr 702 was investigated. The results are summarized as follows:

(1) At 20.4% rolling reduction, some tangled dislocations were observed, indicating that crystallographic slip was the predominant deformation mechanism in the early stages of deformation. At 38.9% rolling reduction, a few deformation twins were observed. The dislocation density and the number of twins increased with increasing rolling reduction, while the size of the dislocation cells decreased. At 71.0% rolling reduction, the microstructure exhibited a fine lamellar structure and deformation twins with wavy boundaries. In addition, the deformation microstructure was heterogeneous, depending on grain orientation.

(2) The initial texture of the Zr 702 plate consisted of a basal fiber component. During the rolling, the strength of the basal fiber first decreased and then increased with increasing rolling reduction. The maximum position of the basal texture changed from the $<2\bar{1}\bar{1}0>$ orientation in the initial state to the $<10\bar{1}0>$ orientation in the 70% rolled state.

(3) The cold-rolled Zr 702 sheets were fully recrystallized after being annealed at 550°C for 1 h. The recrystallization temperature and the size of the recrystallized grains decreased with increasing rolling reduction. A larger rolling reduction resulted in a higher grain growth rate when the annealing temperature increased from 550°C to 700°C. At 700°C, the size of recrystallized grains slightly decreased with increasing rolling reduction.

(4) The recrystallization texture of the cold-rolled sheets was characterized by a major basal fiber and a minor $\{01\bar{1}3\}<2\bar{1}\bar{1}0>$ component. The strength of the recrystallization texture increased with increasing rolling reduction.

Acknowledgements

This work was financially supported by the National Basic Research and Development Program of China (No. 2010CB731606).

References

[1] R.A. Murgatroyd and A. Rogerson, An assessment of the influence of microstructure and test conditions on the irradiation growth phenomenon in zirconium alloys, *J. Nucl. Mater.,* 90(1980), No. 1-3, p. 240.

[2] V. Fidleris, The effect of cold-work and stress-relieving on the irradiation growth behaviour of zirconium alloys, *J. Nucl. Mater.*, 46(1973), No. 3, p. 356.

[3] E.F. Ibrahim, In-reactor tubular creep of Zircaloy-2 at 260 to 300°C, *J. Nucl. Mater.*, 46 (1973), No. 2, p. 169.

[4] R.A. Holt, Recovery of cold-work in extruded Zr–2.5wt%Nb, *J. Nucl. Mater.*, 59(1976), No. 3, p. 234.

[5] C.E.L. Hunt and E.M. Schulson, Recrystallization of zircaloy-4 during transient heating, *J. Nucl. Mater.*, 92(1980), No. 2-3, p. 184.

[6] Y.B. Chun, S.K. Hwang, M.H. Kim, S.I. Kwun, and S.W. Chae, Effect of Mo addition on the crystal texture and deformation twin formation in Zr-based alloys, *J. Nucl. Mater.*, 295(2001), No. 1, p. 31.

[7] M.K. Kumar, I. Samajdar, N. Venkatramani, G.K. Dey, R. Tewari, D. Srivastava, and S. Banerjee, Explaining absence of texture development in cold rolled two-phase

Zr–2.5wt%Nb alloy, *Acta Mater.*, 51(2003), No. 3, p. 625.

[8] K.Y. Zhu, D. Chaubet, B. Bacroix, and F. Brisset, A study of recovery and primary recrystallization mechanisms in a Zr–2Hf alloy, *Acta Mater.*, 53(2005), No. 19, p. 5131.

[9] N. Dewobroto, N. Bozzolo, P. Barberis, and F. Wagner, On the mechanisms governing the texture and microstructure evolution during static recrystallization and grain growth of low alloyed zirconium sheets (Zr702), *Z. Metallkd.*, 97(2006), No. 6, p. 826.

[10] Y.S. Seo, Y.B. Chun, and S.K. Hwang, A 3D Monte-Carlo simulation study of recrystallization kinetics in Zr with hypothetical stored energy gradients, *Comput. Mater. Sci.*, 43(2008), No. 3, p. 512.

[11] F. Gerspach, N. Bozzolo, and F. Wagner, About texture stability during primary recrystallization of cold-rolled low alloyed zirconium, *Scripta Mater.*, 60(2009), No. 4, p. 203.

[12] C. Vanitha, M. Kiran Kumar, G.K. Dey, D. Srivastava, R. Tewari, and S. Banerjee, Recrystallization texture development in single-phase Zircaloy 2, *Mater. Sci. Eng. A*, 519(2009), No. 1-2, p. 51.

[13] Y.I. Jung, M.H. Lee, H.G. Kim, J.Y. Park, and Y.H. Jeong, Behavior of a recrystallization in HANA-4 and HANA-6 zirconium-based alloys, *J. Alloys Compd.*, 479(2009), No. 1-2, p. 423.

[14] J.H. Chung, Development of thermomechanical processing method to enhance twinning in commercially pure Zr, *Scripta Mater.*, 61(2009), No. 2, p. 161.

[15] B.K. Kad, J.M. Gebert, M.T. Perez-Prado, M.E. Kassner, and M.A. Meyers, Ultrafine-grain-sized zirconium by dynamic deformation, *Acta Mater.*, 54(2006), No. 16, p. 4111.

[16] B.S. Lee, M.H. Kim, S.K. Hwang, S.I. Kwun, and S.W. Chae, Grain refinement of commercially pure zirconium by ECAP and subsequent intermediate heat treatment, *Mater. Sci. Eng. A*, 449-451(2007), p. 1087.

[17] O. Castelnau, H. Francillette, B. Bacroix, and R.A. Lebensohn, Texture dependent plastic behavior of Zr 702 at large strain, *J. Nucl. Mater.*, 297(2001), No. 1, p. 14.

[18] Y.B. Chun, S.H. Yu, S.L. Semiatin, and S.K. Hwang, Effect of deformation twinning on microstructure and texture evolution during cold rolling of CP-titanium, *Mater. Sci. Eng. A*, 398(2005), No. 1-2, p. 209.

[19] L. Jiang, M.T. Pérez-Prado, P.A. Gruber, E. Arzt, O.A. Ruano, and M.E. Kassner, Texture, microstructure and mechanical properties of equiaxed ultrafine-grained Zr fabricated by accumulative roll bonding, *Acta Mater.*, 56(2008), No. 6, p. 1228.

[20] M.H. Yoo and C.T. Wei, Slip modes of hexagonal-close-packed metals, *J. Appl. Phys.*, 38(1967), No. 11, p. 4317.

[21] A. Akhtar, Compression of zirconium single crystals parallel to the *c*-axis, *J. Nucl. Mater.*, 47(1973), No. 1, p. 79.

[22] H. Numakura, Y. Minonishi, and M. Koiwa, $<\bar{1}\ \bar{1}\ 23>\{10\bar{1}\ 1\}$ slip in zirconium, *Philos. Mag. A*, 63(1991), No. 5, p. 1077.

[23] R.J. McCabe, E.K. Cerreta, A. Misra, G.C. Kaschner, and C.N. Tomé, Effects of texture, temperature and strain on the deformation modes of zirconium, *Philos. Mag. A*, 86(2006), No. 23, p. 3595.

[24] I.J. Beyerlein and C.N. Tomé, A dislocation-based constitutive law for pure Zr including temperature effects, *Int. J. Plast.*, 24(2008), No. 5, p. 867.

[25] H. Francillette, B. Bacroix, M. Gasperini, and J.L. Bechade, Grain orientation effects in Zr702α polycrystalline samples deformed in channel die compression at room temperature, *Acta Mater.*, 46(1998), No. 12, p. 4131.

[26] A. Akhtar and A. Teghtsoonian, Plastic deformation of zirconium single crystals, *Acta Metall.*, 19(1971), No. 7, p. 655.

[27] J.L. Martin and R.E. Reed-Hill, A study of basal slip kink bands in polycrystalline zirconium, *Trans. AIME*, 230(1964), p. 780.

[28] D. Bhattacharyya, E.K. Cerreta, R. McCabe, M. Niewczas, G.T. Gray III, A. Misra, and C.N. Tomé, Origin of dislocations within tensile and compressive twins in pure textured Zr, *Acta Mater.*, 57(2009), No. 2, p. 305.

[29] M.H. Yoo and J.K. Lee, Deformation twinning in h.c.p. metals and alloys, *Philos. Mag. A*, 63(1991), No. 5, p. 987.

[30] B. Radhakrishnan, S.B. Gorti, G.M. Stoica, G. Muralidharan, A.D. Stoica, X.L. Wang, E.D. Specht, E. Kenik, and T. Muth, Mesoscale modeling and validation of texture evolution during asymmetric rolling and static recrystallization of magnesium alloy AZ31B, *Metall. Mater. Trans. A*, 43(2012), No. 5, p. 1509.

[31] M.H. Li, M. Ma, W.C. Liu, and F.Q. Yang, Recrystallization behavior of cold-rolled Zr 702, *J. Nucl. Mater.*, 433(2013), No. 1-3, p. 6.

[32] R.D. Doherty, Recrystallization and texture, *Prog. Mater. Sci.*, 42(1997), p. 39.